JATIS Journal of Astronomical Telescopes, Instruments, and Systems

RESEARCH PAPER

High-bandwidth, compact fine-steering mirror design for the CubeSpec space mission

Jeroen De Maeyer,[a,*] Gert Raskin,[b] Bart Vandenbussche,[b] and Dirk Vandepitte[a]
[a]KULeuven, Department of Mechanical Engineering, Heverlee, Belgium
[b]KULeuven, Institute of Astronomy, Heverlee, Belgium

ABSTRACT. The primary goal of the CubeSpec mission is to show the feasibility of high-resolution optical astronomical spectroscopy from a small and cheap space platform. In its showcase mission, this 12U CubeSat space telescope will observe a time series of spectra of multiple β-Cephei pulsators. The inner structure of these stars can be derived from the spectral line profile variations. The optical payload, composed of an off-axis Cassegrain telescope and compact optical bench with a spectrograph, occupies half of the available volume and measures $\sim 10 \times 20 \times 30$ cm^3. During the observations, the star should be imaged on the spectrograph entrance slit of 20×50 μm ($2.6'' \times 6.5''$) for at least 80% of the time to reach the sensitivity required. This leads to strict pointing requirements for the mission that cannot be met with the attitude determination and control system (ADCS) architecture of CubeSats. Therefore, we implemented a second control loop, based on a high-precision pointing platform (HPPP) that relies on its own sensor and actuator to measure the pointing error to a few arcsec accuracy and apply the proper compensation. In contrast to the ADCS, the HPPP does not change the spacecraft attitude but changes the optical path within the payload to project the image of the star inside the spectrograph slit. This paper describes the mechanical design of the fine-steering mirror (FSM), one of the key components of the HPPP. The design fits within the tight volume constraints of CubeSats and CubeSpec in particular and satisfies all mechanical challenges defined by the system dynamics and launch conditions. The three degrees of freedom design has a peak-to-peak tip/tilt range larger than 7 mrad along two tip/tilt axes and a first structural mode at 810 Hz while meeting the dimensional constraints. Especially the combination of a large actuated mirror with the small dimensions of the mechanism is a step forward with respect to commercially available FSM mechanisms, which typically do not match the CubeSat volume constraints. The concept can be easily scaled to various applications with different sets of requirements at a reasonable cost using commercial-of-the-shelf components.

© The Authors. Published by SPIE under a Creative Commons Attribution 4.0 International License. Distribution or reproduction of this work in whole or in part requires full attribution of the original publication, including its DOI. [DOI: 10.1117/1.JATIS.10.3.034005]

Keywords: fine-steering mirror; compact; actuated mirror; finite element method analyses; CubeSpec

Paper 24030G received Mar. 29, 2024; revised Jul. 12, 2024; accepted Jul. 30, 2024; published Aug. 21, 2024.

1 CubeSpec Mission

The primary goal of CubeSpec is to show the feasibility of high-resolution optical spectroscopy from a CubeSat platform. Such an economical platform opens up new possibilities for dedicated missions acquiring uninterrupted high-quality spectral time series from a limited set of bright

*Address all correspondence to Jeroen De Maeyer, jeroen.demaeyer1@kuleuven.be

stars. Up to now, the prohibitively high cost of spectroscopic missions rendered this unfeasible. Similar observations from ground-based telescopes inevitably suffer from time gaps that compromise the quality of the data. CubeSpec is a European Space Agency (ESA) in-orbit demonstration (IOD) mission, funded by the Belgian Science Policy Office (BELSPO). It will observe the pulsations of various β-Cephei stars by monitoring the variations in the profile of the absorption lines in their spectra regularly over the time span of one to several months. Through the technique of asteroseismology, we can derive the inner structure of the observed stars from these pulsations. Mission science requirements are summarized as follows:[1]

1. A spectral resolving power of at least $R > 50000$
2. Signal-to-noise (S/N) ratio above 200 in the individual spectra of stars with a visual magnitude (m_V) of 0 to 4, to allow the identification of line profile variations which are of the order of only a few percent of the light continuum
3. Sufficient sampling of five to 10 observations during one pulsation period, typically between 8 and 24 h
4. Integration times shorter than 15 min to avoid temporal smearing of the line profile deformations
5. Regular observations of the same stars over a period of at least 100 days.

Figure 1 shows an artist's impression of the 12U CubeSpec spacecraft, measuring roughly $20 \times 20 \times 34$ cm^3. Six units (6 U or $10 \times 20 \times 30$ cm^3) are allocated to the optical payload and baffle, whereas the other 6 U are occupied by the payload electronics and platform hardware. The telescope itself always points to deep space, and direct illumination by the sun is avoided. The payload position deep inside the spacecraft maximizes the sun exclusion angle. A radiator positioned between the two brown Earth and Sun shields disposes of the heat generated by the science sensor.

The optical payload consists of a diffraction-limited off-axis Cassegrain telescope, with a focal length of 1600 mm and a 184×86 mm^2 aperture, and a high-resolution echelle spectrograph,[2] observing the wavelength range from 420 to 620 nm in a single exposure. A crucial component of the spectrograph is the entrance slit, indicated in Fig. 2. During every 15-min observation, light should pass at least 80% of the time through this slit that measures 20×50 μm or 2.6" $\times$ 6.5" on the sky to reach the required S/N ratios. The requirement translates into a maximum absolute pointing error (APE) of 1.3" $\times$ 3.25" (half cone angle) along the telescope cross-boresight axes, the relative pointing error (RPE) along those axes is less important.[3] Unfortunately, current state-of-the-art attitude determination and control systems (ADCS) onboard the large majority of CubeSats have an APE in the order of 100",[4] which by itself does not meet the specification. In specific cases, better performance can be obtained for example in the Asteria mission with the Blue Canyon XACT ADCS with a 10" RPE along the cross-boresight axes over a 20-min observation window.[5] To cope with the ADCS limitations and pointing

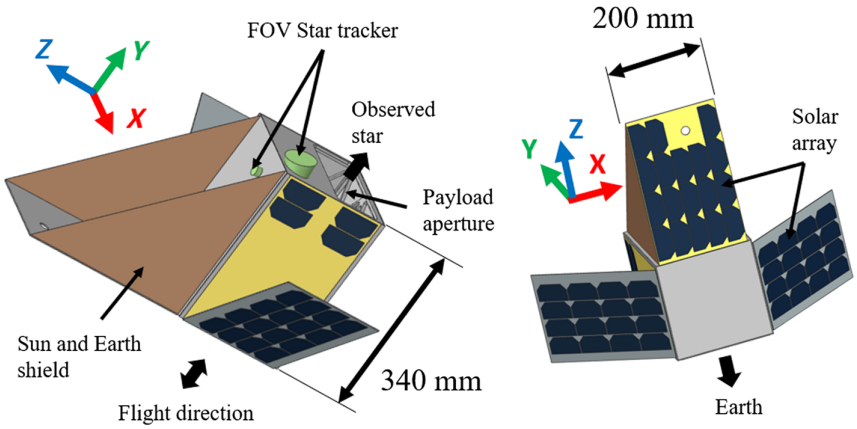

Fig. 1 Artist's impression of the CubeSpec spacecraft. The star tracker field of views is indicated with green cones, and the brown triangles indicate the Sun and Earth shields.

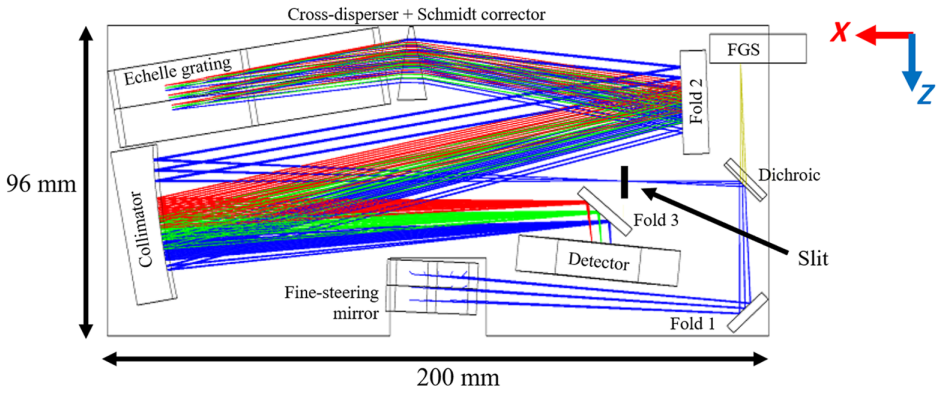

Fig. 2 Lay-out of the CubeSpec optical bench. The distance between the fine-steering mirror (FSM) and slit exactly matches the distance between FSM and FGS.

requirements, CubeSpec deploys a second control stage called the high-precision pointing platform (HPPP) that actively adapts the optical path within the satellite without affecting the spacecraft's attitude. The second control layer actively corrects for residual ADCS pointing errors that translate into a movement of the star image on the slit. The main components of the additional control layer are a fine-steering mirror (FSM), a fine guidance sensor (FGS), and a controller implemented on an FPGA.[3] CubeSpec's HPPP only compensates for cross-boresight errors as the pointing requirement along the boresight axis with an APE of 0.2 deg (half cone angle), and an RPE of 180″ (half cone angle) can be met with the ADCS.[3] A similar technique has already been shown on the Asteria mission[5] with a translation stage moving the image sensor, instead of an FSM. The linear stroke of the FSM at the sensor $\Delta_{FGS} = \theta_{FSM} x_{sp}$ is determined by the FSM angular stroke (θ_{FSM}), as well as by the distance between the FSM and sensor (x_{sp}). Due to the lever effect the FSM can compensate a much wider range of pointing errors for the same actuator stroke (Δ_{act}) compared with a translation stage ($\Delta_{FGS} = \Delta_{act}$). Moreover, for CubeSpec, the injection point of the spectrograph is fixed in space. Moving the slit to center the spot within the slit would not lead to improved data quality as the injection in the spectrograph would happen at the wrong location in this case.

A dichroic beamsplitter located on the optical bench divides the collected light between the FGS and the spectrograph, where wavelengths not of interest for the science observations are redirected to the FGS. Reference 6 provides a detailed discussion of the optical design. The distance between FGS and FSM exactly matches the distance between slit and FSM such that a 1-to-1 relation applies between a shift on both the FGS and on the slit, as illustrated in Figs. 2 and 3. The limited volume and the fact that a large optical surface should be tip/tilted require a custom mirror design that complies with all requirements in Table 1. To avoid coupling between the spacecraft and launcher, launch authorities impose a minimum value (135 Hz) for the first structural mode. However, for its operational life, it is beneficial that the first structural mode is

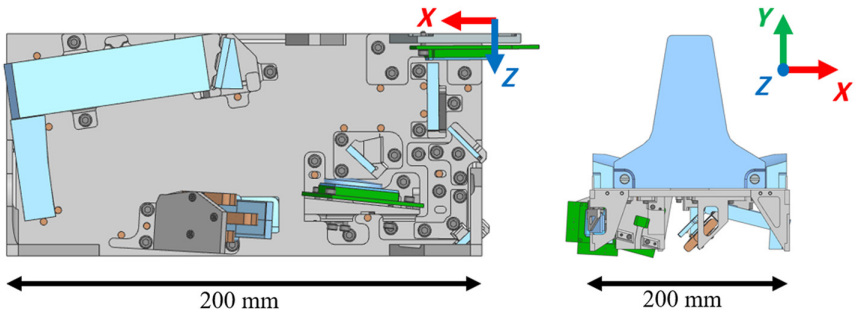

Fig. 3 Preliminary design of the CubeSpec optical science payload, the long side of the bench measures ~200 mm, and the short side 96 mm. Following CubeSat design limits the short side cannot exceed 100 mm, neglecting spacecraft structural panels. The FSM is visible at the lower side and the middle of the optical bench.

Table 1 FSM design requirements.

Parameter	Unit	Value
Mirror dimensions		
Mirror width	mm	16
Mirror length	mm	36
Max. mirror deformation	nm	≤75
Mass	gram	<6
Mechanism		
Degrees of freedom	—	≥2
Mech. stroke (peak-to-peak)	mrad	≥6
First mode (launcher)	Hz	>135
First mode (desired)	Hz	>500
Lifetime	year	0.5
Actuator limits		
Input voltage	V	≤80

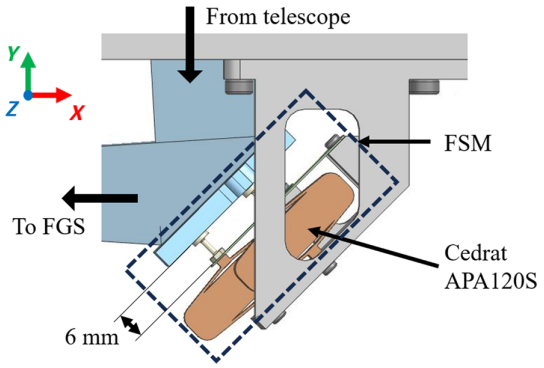

Fig. 4 Detail of the FSM position within the CubeSpec payload. Light comes in from the secondary mirror of the off-axis Cassegrain telescope (top of the figure) and is reflected towards the rest of the optical bench (left side of the mirror).

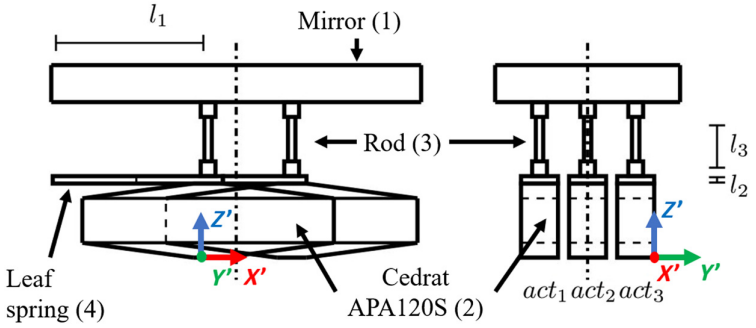

Fig. 5 FSM design concept with (1) the mirror, (2) the actuator, (3) the elastic element, and (4) the leaf spring. Design parameters are indicated in the figure, and the following dimensions apply to the implemented FSM: $l_1 = 15.4$ mm, $l_2 = 0.3$ mm, $l_3 = 4$ mm, and rod diameter = 1.2 mm.

even higher to improve the dynamic mirror steering. Therefore, the value as mentioned in the table is the absolute minimum requirement to avoid a hold down and release mechanism (HDRM) during launch. The HPPP has a sampling frequency of 35 Hz, but the FSM has a dedicated feedback loop that runs at 1000 Hz to reduce FSM settling time. A first structural FSM mode above 500 Hz is desired. With the FSM orientation at 45 deg with respect to the horizontal plane, there is an amplification factor of 2 on the FGS reading, $\Delta_{FGS} = 2\theta_{FSM}x_{sp}$, for an FSM rotation around the short mirror axis but only an amplification of 1, $\Delta_{FGS} = \theta_{FSM}x_{sp}$, for the FSM rotation around the long mirror axis (Figs. 4 and 5).

2 Literature Review

FSMs have a broad application field ranging from laser beam steering in for example laser communication,[7] laser interferometers,[8] or image stabilization for Earth observation[9] and astronomy (e.g., JWST[10]), each of them with its own specific set of requirements. Reference 11 gives an extensive overview of different FSM configurations together with some applications in space missions. Laser beam communication takes advantage of small highly dynamic mirrors to have good response times, whereas imaging applications often require the movement of larger and heavier mirrors, leading to higher load-bearing mechanisms with longer response times. It turns out that none of these FSM designs matches the CubeSat volume constraints. A non-exhaustive overview of the most important FSM selection criteria is given below:

- Degree of freedom (DoF): DoFs in which the mirror can be moved, ranging from two (tip/tilt) or three (tip/tilt + translation) to six for hexapod designs. Two DoF mirrors often have a ball or flexural joint connecting the mirror and mount to increase the stiffness.
- Actuation: Transform a steering signal, typically a voltage, into mirror movement. Compact designs commonly use voice coil[7,9,12,13] or piezo-electric actuators such as piezo-stack,[14,15] piezo-walkers,[8,16] or amplified piezo-actuators.[17] Voice coil actuators require in general more power for the same stroke compared to the piezo-electric ones.
- Size: Mechanism and mirror size are important. The larger the mirror, the lower the eigenfrequency of the mechanism's first structural mode due to the increased actuated mass.
- Bandwidth: (Closed loop) control bandwidth of the FSM. A higher control bandwidth allows for compensation of higher frequency temporal disturbances.

3 FSM Design Concept

To minimize design complexity, our design combines commercial-of-the-shelf (COTS) components when available with custom metal parts that are manufactured with standard three or five-axis milling machines. The main FSM components are illustrated in Fig. 5.

1. The mirror to be tip/tilted, manufactured from a low-expansion optical material such as fused silica, Zerodur, or Cordierite.
2. Three actuating elements converting a steering voltage in a mirror tip/tilt or translation. The literature review mentions that the two common types of actuators are piezo and voice coil actuators. However as voice coil actuators have a cylindrical shape for our applications amplified piezo actuators are more suited thanks to their rectangular shape and limited width with the additional advantage of lower power consumption. The selected compact Cedrat APA120S amplified piezo actuators have a 120-μm stroke and are equipped with strain gauges attached to the piezo stacks to linearize their response with appropriate feedback control.[18] Although two actuators are sufficient for tilt control along two perpendicular axes, the three actuator layout adds thermal symmetry and result in better thermal performance with a more even deformation pattern.
3. Elastic elements connecting mirrors and actuators. Two design parameters, the rod length (l_3) and diameter, determine the stiffness and the required actuator force and stress within the structure.
4. Three leaf springs connecting the top of the actuators with the rest of the structure: thickness $l_2 = 0.3$ mm, length $l_1 = 15.4$ mm, and width = 5 mm.
5. An epoxy (glue) layer to connect the elastic elements with the mirror (thickness = 0.1 mm).

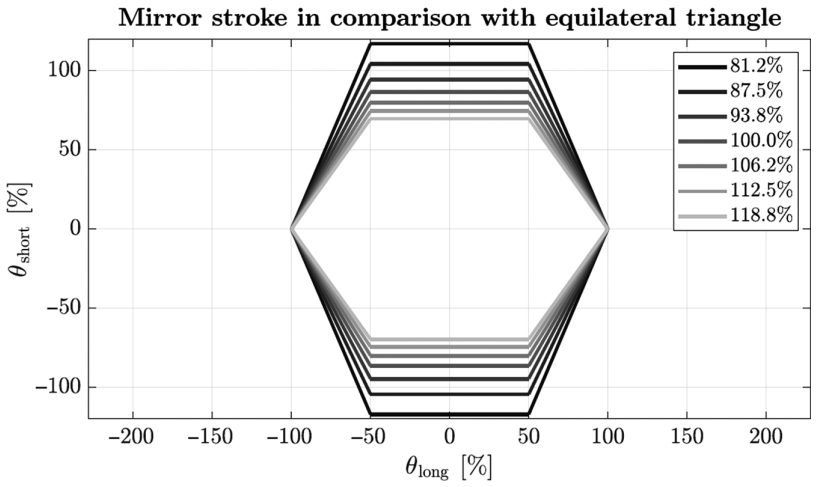

Fig. 6 Theoretical FSM stroke compared to an equilateral triangle (100%). Values expressed in function of the length of the legs compared to the triangle base and results in function of the maximal stroke along the long mirror axis.

Actuators are mounted on the vertices of an equilateral triangle with a side length of 16 mm, which maximally exploits the available volume width. Figure 6 shows the theoretical stroke as a function of triangle height expressed in percentage with respect to the equilateral solution. A large triangle height would increase the first structural eigenmode but decrease the stroke (as indicated by the figure) and vice versa. Stiffness along short [θ_{short}, rotation along the shortest mirror side (Y')] and long [θ_{long}, rotation along the longest mirror side (X')] mirror axes differ with the highest value for the latter one. Due to the over-constrained construction, the mirror surface deforms when the FSM is actuated, which is partly mitigated by the elastic rods.

Numerical simulations using Siemens NX2206 Finite Element (FE) software (Fig. 7) show a relatively low eigenmode located at ± 455 Hz, for a design without a leaf spring. This first mode corresponds to an actuator tilt along the short mirror axis. The design of Fig. 5 offers a solution that limits this tilt, and it increases the first mode frequency and improves the dynamic properties. Finally, it also reduces the required actuator force without compromising the overall performance. As actuator forces and strokes are coupled within piezoelectric actuators, they cannot provide maximum stroke and force at the same time.[19] Hence, a trade-off between both has to be made with lower actuator forces resulting in larger FSM strokes. Table 3 shows that the required actuator force increases with rod diameter in a nonlinear way. The force increase in case of a larger rod diameter (proportional to the fourth power of the diameter) is much larger compared to the increase in case of a reduced rod length (inversely proportional to the third power of the length). Therefore, a smaller rod diameter is preferred over a larger rod length. An added advantage of reduced diameters is the decrease in rod stress due to bending, improving the cyclic fatigue life of the structure.

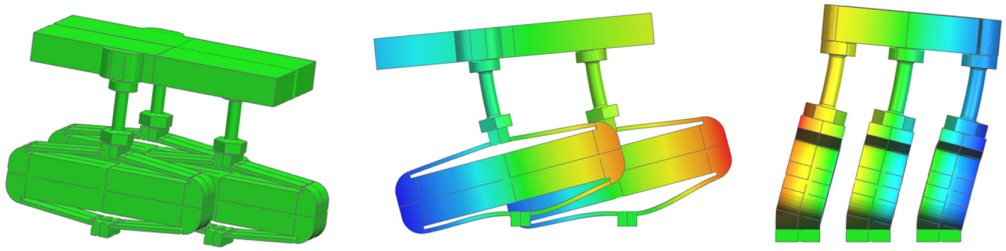

Fig. 7 From left to right: undeformed FSM, first (455 Hz) and second (486 Hz) structural eigenmode of a design without leaf springs ($l_3 = 6$ mm and rod diameter = 1.8 mm). The same FE approach as described by Sec. 4.1 is applied.

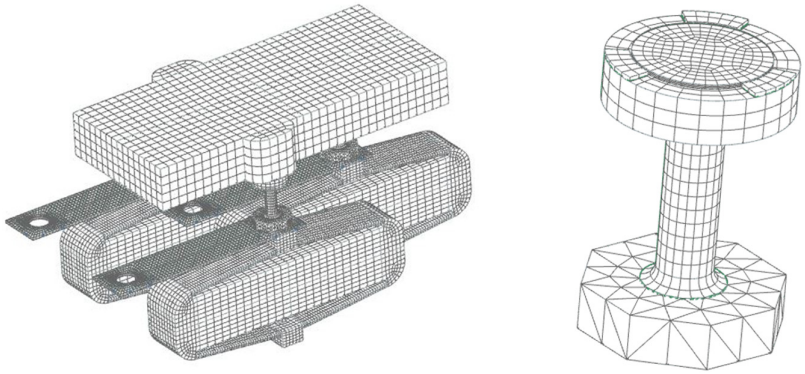

Fig. 8 Finite element model (FEM) of the whole structure (left) and of one of the rods (right). The epoxy layer on top of the rod has been modeled with four elements in the thickness.

4 FE-Based Stroke and Eigenmode Estimations

FE simulations verify a broad range of design parameters without the need for a physical implementation. The high required bandwidth in combination with the large actuated mirror within the dimensional limits imposes some design challenges. FE analysis is extensively used to match the conflicting requirements in the best way possible.

4.1 FE Model

The Siemens NX-Nastran environment is used to run static simulations (solution sequence 101) and normal mode (solution sequence 103) analyses to locate structural excitation modes and verify the effect of different design parameters. Figure 8 and Table 2 provide details of the model in terms of material and element parameters. Three cylindrical elastic epoxy layers connect the mirror and actuator rods in the FE model. The FSM mechanism is fixed in all six degrees of freedom at the interfaces between the mechanism and optical payload. All simulations neglect actuator preload in the amplified piezo actuators. Although rod and leaf spring materials are not limited to aluminum, the limited Young's modulus (72.3 GPa) of an Al-7075 alloy is a good compromise between actuator force, bending stress, and lifetime.

4.2 *Sensitivity Analysis on Key Design Parameters*

Stiffness increases with decreasing rod length (l_3) and increasing rod diameter as shown in Table 3. However, the required actuator forces increase drastically with diameter making it a less influential design parameter. Although both factors have an influence, differences are small as all evaluated designs have a first mode between 935 and 1024 Hz for the 4 mm mirror and

Table 2 FE FSM simulation model parameters. Unless explicitly indicated in the text, all FE models apply the element size as summarized in the table.

Component	Material	Element type	Element size [mm]
Actuator shell	Springsteel	CHEXA20	0.25
Actuator (piezo)	Piezo material	CHEXA20	0.9
Rod	Aluminum	CHEXA20	0.2 to 0.3
—	Aluminum	CTETRA10	0.87
Leaf spring	Aluminum	CQUAD8	0.4
Glue pad	2216 B/A (3M)	CHEXA20	0.25 (4 layers)
Mirror	Zerodur	CHEXA20	1
—	Zerodur	CTETRA10	0.4

Table 3 FE FSM results in function of rod diameter, length, and mirror height. l_1 equals 15.4 mm for all simulations. Forces are calculated for an FSM 3 mrad rotated along the short mirror axis and 1.6 mrad rotated along the long mirror axis.

l_3	d_{rod}	Frequency [Hz]		Actuator force [N]	
mm	mm	4 mm mirror	5 mm mirror	4 mm mirror	5 mm mirror
6	1.8	997.31	899.39	3.274	3.280
6	1.5	970.31	882.15	1.803	1.805
6	1.2	935.42	839.73	0.861	0.862
5	1.2	970.12	886.65	0.887	0.998
4	1.2	998.51	918.70	1.195	1.196
3	1.2	1024	947.57	1.507	1.508

839 and 947 Hz for the 5 mm mirror. A thicker mirror lowers the first mode but has almost no influence on the required actuator forces. All values are theoretical values based on nominal design data, real implementations are never perfect and may show slightly deviating eigenmode values with respect to the nominal FE simulations (see Sec. 5.3). The remainder of the paper further elaborates on the design combining 4-mm long rods with a 1.2-mm diameter.

4.3 *Detailed Performance Analysis of Selected Design*

The first FSM mode shape of the design with a leaf spring is similar to the one without as they both correspond to a rotation around the short mirror axis. However, for the design with leaf springs, this mode is located at 998 Hz instead of 400 Hz. The second mode (1077 Hz) bends and shifts the structure around the long mirror axis, whereas the third mode (1187 Hz) corresponds to a translation along the optical mirror axis, as shown in Fig. 9. Table 4 shows that most modal mass is located at frequencies well above the envisaged FSM sampling rate with mode 3 containing almost all modal mass along the Z' axis. The modal mass along the X' and Y' axes is distributed over multiple modes with mode contributions up to 40%, and the lowest mode (998 Hz) shown in Fig. 9 has a limited contribution.

FE analyses with a refined mirror mesh predict the (static) mirror deformation in one of the extreme FSM positions as shown in Fig. 10. The 0.3-mm element size shows more detail in the deformed mirror deformation pattern and improves the results. Maximum mirror deformation of 88 nm peak-to-peak is outside the requirement set by Table 1. However, if only the clear aperture of the mirror is taken into account, which starts 2 mm from the edge, the maximum mirror deformation of 71 nm falls within requirements. Although within requirements, the margin is small, mirror substrates with higher Young's moduli (for example Cordierite) increase the margin with negligible change in dynamic properties.

Figure 11 shows that peak stress occurs in the leaf spring and rod; however, for the required tip/tilt angles, stress (29.2 MPa for aluminum parts, 1 MPa for glue pads) is well below material

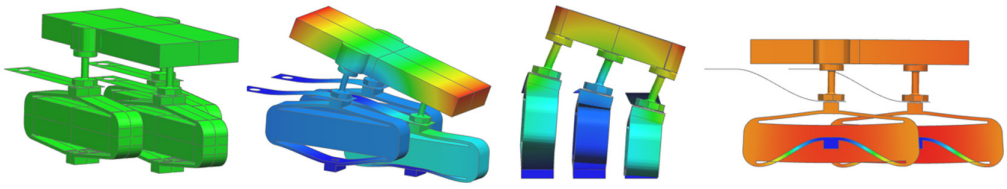

Fig. 9 Modes as calculated by the FE analyses for the design with 4-mm long rods and a diameter of 1.2 mm. From left to right: undeformed state, first mode at 998 Hz, second mode at 1077 Hz, and third mode at 1187 Hz.

Table 4 Modes as calculated by the FE analysis with the highest modal mass or as visualized in Fig. 9.

Mode	Frequency (Hz)	Modal mass X' (%)	Modal mass Y' (%)	Modal mass Z' (%)
1	998	2.4	0.0	0.0
2	1077	0.0	16.0	0.0
3	1187	0.0	0.0	97.1
4	1484	0.0	27.2	0.0
6	1858	3.55	0.0	0.0
8	2250	0.0	34.3	0.0
14	3420	30.3	0.0	0.0
27	12630	40.2	0.0	0.0

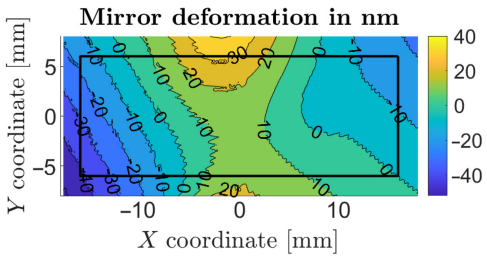

Fig. 10 Mirror deformation as calculated by the FE analysis. The mirror is 3 mrad rotated along the short mirror axis and 1.6 mrad along the long mirror axis. The black rectangle indicates the useful mirror area. All deformations are measured along the optical axis of the mirror.

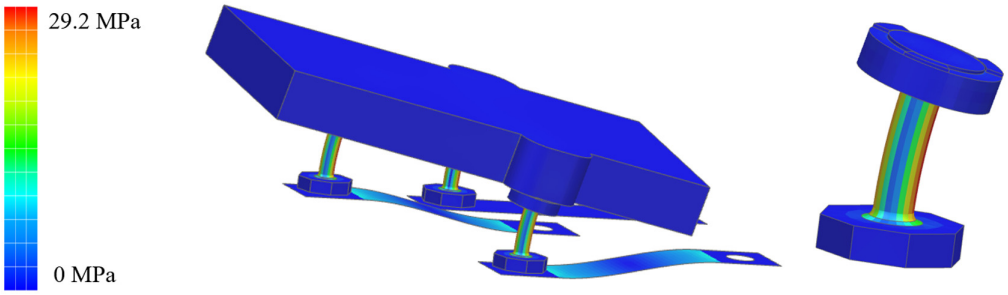

Fig. 11 Elemental Von Mises stress distribution in the FSM mechanism and the rod; red values correspond to stress values of 29.2 MPa. Mirror tilt of 3 mrad along the short mirror axis and 1.6 mrad along the long mirror axis.

limits. A 0.3-mm edge radius between the rod neck and foot avoids stress concentrations at those locations and limits peak stress.

5 Stroke and Eigenmode Measurements

FE models and FSM performance are further verified by a mechanically equivalent model of the design as described in the previous section. An aluminum dummy mirror replaces the Zerodur one in the test set-up as shown in Fig. 12. Aluminum is easier to manufacture, and due to its similar density an ideal replacement, the metallic surface also simplifies capacitive measurements. In contrast to the simulations, where the rods are connected with a glue layer

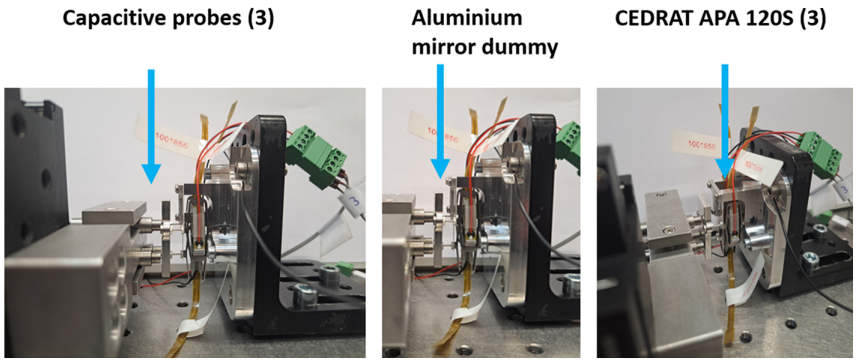

Fig. 12 FSM breadboard with aluminum dummy mirror. Three capacitive probes are visible on the left, and the mirror assembly on the right.

(3M 2216 B/A) to the mirror, the mirror is fixed between a rod and a nut without any application of glue.

5.1 Description of Test Set-Up

Figure 13 illustrates the test set-up, and although actuator voltages up to 150 V are feasible, within our application, they are limited to 80 V due to constraints of onboard electronics. Steering voltages between 0 and 8 V are sent to the PI E831.03 amplifiers (amplification factor of 10) connected to three Cedrat APA120S actuators to tip/tilt or translate the mirror along its optical axis. Specific tests determine the type of steering signal: (quasi-)static measurements use a continuous square wave, whereas dynamic measurements require a sine (sweep) signal.

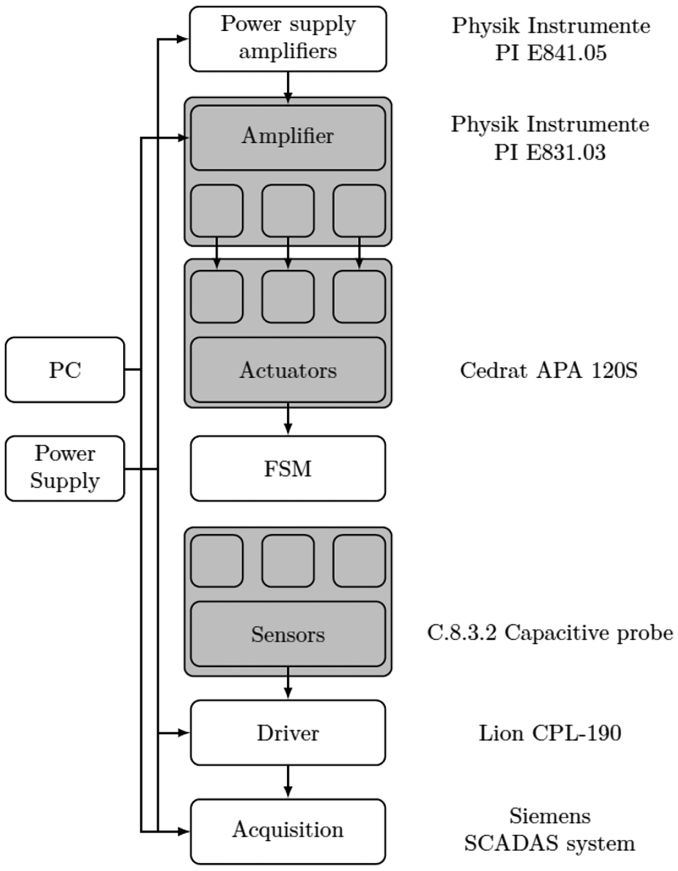

Fig. 13 Test set-up used to verify FEM and FSM performance. Each of the actuators has its own amplifier, and each of the capacitive probes has its own Lion CPL-190 card as illustrated in the figure.

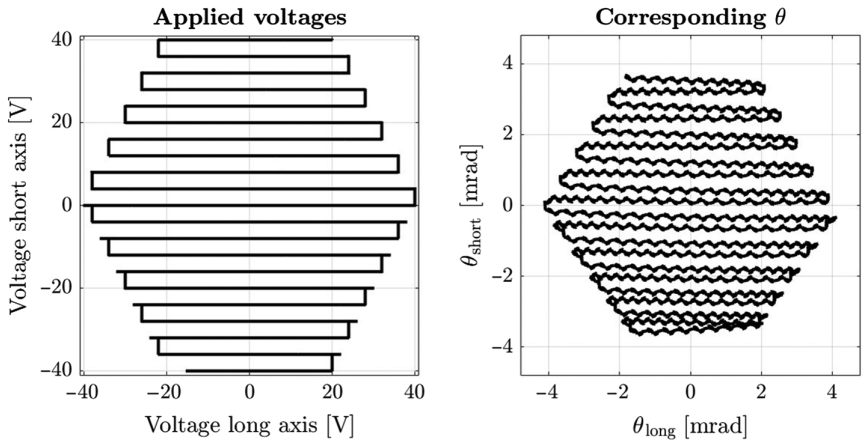

Fig. 14 Measured FSM stroke (right). All actuators received a nominal voltage of 40 V (U_{trans}) in which the voltages as shown in the left figure ($U_{\theta,\text{short}}$, $U_{\theta,\text{long}}$) are superimposed following the definitions of Eq. (1).

Three non-colinear capacitive probes remotely measure different points distributed over the mirror surface, fitting a plane through those three points converts the measurements into tip/tilt angles and mirror translation. A Siemens SCADAS data acquisition system (VIBCO frame equipped with VD8E and analog output card) in combination with Siemens Testlab (version 2206) software measures and synchronizes the applied input voltages and capacitive output signal for post-processing.

5.2 *Stroke and Hysteresis*

The maximum FSM stroke envelope has a hexagonal shape as shown in Fig. 14, which shows both applied voltages and corresponding FSM tip/tilt angles. The actuator voltages U_1, U_2, and U_3 are calculated from the control voltages $U_{\theta,\text{short}}$ (rotation along the short mirror axis), $U_{\theta,\text{long}}$ (rotation along the long mirror axis), and U_{trans} (mirror translation along the optical axis) as follows:

$$\begin{aligned} U_1 &= U_{\theta,\text{long}} - U_{\theta,\text{short}}/2 + U_{\text{trans}} \\ U_2 &= U_{\theta,\text{short}} + U_{\text{trans}} \\ U_3 &= -U_{\theta,\text{long}} - U_{\theta,\text{short}}/2 + U_{\text{trans}}. \end{aligned} \tag{1}$$

When U_2 reaches its maximum value, U_1 and U_3 still have some margin to tilt the mirror. The measured angles in the range −4.11 to 4.08 mrad for θ_{long} and from −3.63 to 3.63 mrad for θ_{short} are well within requirements. Strokes are slightly lower than the theoretical values based on geometry and an actuator gain of 0.8667 μm/V, $\theta_{\text{long}} = 4.3$ mrad and $\theta_{\text{short}} = 3.8$ mrad.

Hysteresis is one of the drawbacks of (amplified) piezo-actuators, which complicates the control of piezo-driven mechanisms and is clearly present in the FSM (see Fig. 15). The hysteresis phenomenon requires proper feedforward or feedback control for accurate positioning. Feedback control also compensates for small coupling between both axes. A coupling-free mechanism would show horizontal lines on the left side of Fig. 15.

5.3 Eigenmodes

Figure 16 illustrates that the first mode corresponds to a rotation along the short mirror axis (the first mode in Fig. 9) as the mode is mainly visible when actuator 2 is excited. Higher modes are harder to distinguish, but there are two around 1000 Hz, one corresponds to the rotation around the long mirror axis and the other one is the translation along the mirror's optical axis. An 18% deviation between the measured (810 Hz) and calculated mode (998 Hz) is observed, but both are well above the minimal required eigenmode, and mode shape resemblance is sufficient for our application, especially with the simplified actuator model.

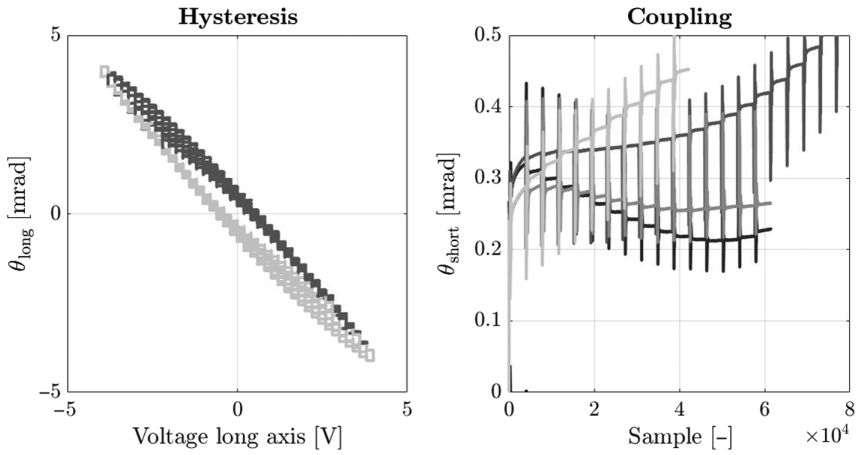

Fig. 15 Measured FSM hysteresis and coupling along θ_{short}. Coupling refers to the unwanted rotation along an axis, whereas the other one is tip/tilted. During measurements, U_{short} is kept constant. Coupling lines are centered such that the first sample coincides with (0,0). The peaks present on the left figure correspond with a change of U_{long}. Every line corresponds with a change of U_{long} from its minimum to maximum value, whereas U_{short} was kept constant at a different voltage.

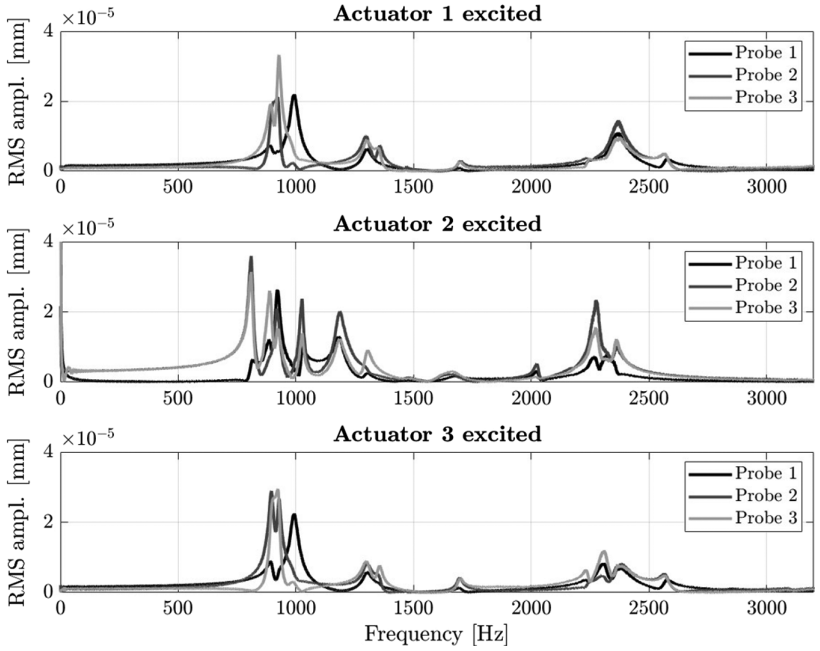

Fig. 16 Measured eigenmodes of the FSM test set-up and actuator set-up as shown in Fig. 5. Every subfigure shows the capacitive probe measurements when one of the actuators was excited with a periodic chirp signal of 0.1 V up to 3200 Hz while the others were at rest. Probe measurements are sampled at 6400 Hz.

6 Conclusions

The CubeSpec FSM design combines Cedrat APA120S actuators with leaf springs and elastic rods. The movement along three DoF (tip/tilt and translation along the optical axis) with 7.2 mrad peak-to-peak tip/tilt performance for an actuator driving voltage of 80 V and mirror surface deformations below 75 nm meet all static requirements. The first structural eigenmode located at 810 Hz complies with launcher requirements and guarantees a sufficient margin for FSM control without exciting the structural mode. With its small volume, large stroke, and large actuated

mirror, it is ideal to fit inside compact optical payloads similar to CubeSpec when COTS solutions are not feasible. As design parameters can be tuned over a broad range, the FSM can be tailored to specific needs. The selection of COTS actuators and elastic elements which may be produced on common milling or turning machines limit the development time and cost.

Disclosures

There is no conflict of interest.

Code and Data Availability

All models and test set-ups in support of the findings of this paper are described within the article. Upon request, they can be shared by contacting the author at jeroen.demaeyer1@kuleuven.be.

Acknowledgments

The authors thank the European Space Agency (ESA) and the Belgian Federal Science Policy Office (BELSPO) for their support of the CubeSpec mission development in the framework of the GSTP program and the Fonds Wetenschappelijk Onderzoek (FWO) for funding the developments of the HPPP concept in the context of the Aqualis project (Grant No. S000719N).

References

1. D. M. Bowman et al., "The CubeSpec space mission, I. Asteroseismology of massive stars from time-series optical spectroscopy: Science requirements and target list prioritisation," *Astron. Astrophys.* **658**, A96 (2022).
2. B. Vandenbussche et al., "CubeSpec–enabling spectroscopy from a CubeSat platform," in *Proc. of the Small Satellites, Syst. and Serv. Symp. (4S)*, Vilamoura (2022).
3. W. De Munter et al., "High precision pointing platform performance simulations for small spacecraft missions," in *Proc. Guidance, Navigation and Control Conf. (GNC)*, Sopot (2023).
4. J. Vandersteen, J. Vennekens, and R. Walker, "Nano- to small satellite pointing errors: limits of performance," in *Proc. of the Small Satellites, Syst. and Serv. Symp. (4S)*, Valetta (2016).
5. C. M. Pong, "On-orbit performance & operation of the attitude & pointing control subsystem on ASTERIA," in *Proc. 32nd Annu. AIAA/USU Conf. on Small Satellites*, Logan (2018).
6. G. Raskin , J. De Maeyer, and B. Vandenbussche et al., "Cubespec: optical payload design," *Proc. SPIE* **12180**, 121802Z (2022).
7. S. Kuiper, W. Crowcombe, and J. Human, et al., "High-bandwidth and compact fine steering mirror development for laser communications," in *Proc. 17th Europena Space Mech. and Tribil. Symp. (ESMAT)*, Hatfield (2017).
8. S. Henein et al., "Flexure-based pointing mechanism with sub-microradian resolution for the laser interferometer space antenna," in *Proc. of the Euspen Internal Conf.*, Delft (2010).
9. T. Shinshi et al., "A fast steering mirror using a compact magnetic suspension and voice coil motors for observation satellites," *Electronics* **9**, 1997 (2020).
10. L. Blackmore et al., "Instrument pointing capabilities: past, present, and future," in *Proc. of AAS Guidance and Control Conf.*, Breckenridge (2011).
11. M. Milaševičius and L. Mačiulis, "A review of mechanical fine-pointing actuators for free-space optical communication," *Aerospace* **11**, 5 (2024).
12. Y. Long et al., "Design of a moving-magnet electromagnetic actuator for fast steering mirror through finite element simulation method," *J. Magn.* **19**, 300–308 (2014).
13. R. Xiao, M. Xu, and S. S. Z. Tian, "Design and wide-bandwidth control of large aperture fast steering mirror with integrated-sensing unit," *Mech. Syst. Signal Process.* **126**, 211–226 (2019).
14. F. M. Tapos et al., "High bandwidth fast steering mirror," *Proc. SPIE* **5877**, 587707 (2005).
15. S. C. Woody and S. T. Smith, "Steering mirror design and dynamic controls for a dual-actuation platform using high-strain actuators," in *Collection of Tech. Pap. - AIAA/ASME/ASCE/AHS/ASC Struct., Struct. Dyn. and Mater. Conf.*, Austin (2005).
16. F. Dubois et al., "Module stepping piezoelectric actuator–a versatile way of micro-positioning actuation," in *Actuator (Conf.)*, Bremen (2016).
17. Z. Jing et al., "Development of a tilt-positioning mechanism driven by flextensional piezoelectric piezoelectric actuators," *Rev. Sci. Instrum.* **87**, 085006 (2016).
18. Cedrat Technologies, "APA120S amplified piezo actuator," [Datasheet] (2022).
19. Cedrat Technologies, "Products catalogue version 5.1," [Catalogue] (2021).

Jeroen De Maeyer is a PhD student at the KULeuven. He received his MS degree in engineering science in 2020 at the same university. His main research area is the pointing improvement of Cube- and SmallSats by adding a second control stage (with its own actuator and sensors) on top of the traditional attitude determination and control systems.

Biographies of the other authors are not available.